Journal Name

ARTICLE TYPE

Cite this: DOI: 00.0000/xxxxxxxxxx

Supporting Information – Intermetallics with sp-d orbital hybridisation: morphologies, stabilities and work-functions of In-Pd particles at the nanoscale

Alexis Front*[a,b], Clovis Lapointe[a,c] and Émilie Gaudry*[a]

Received Date
Accepted Date

DOI: 00.0000/xxxxxxxxxx

S1 Computational details

Table S1 k-mesh and slab thickness z (in number of atomic layer) of each surface orientations and compounds studied

	(hkl)	k-mesh	z
In_3Pd_2	(100)	$10\times8\times1$	13
	(001)	$10\times10\times1$	13
	(110)	$8\times6\times1$	13
	(101)	$10\times6\times1$	13
InPd	(100)	$15\times15\times1$	15
	(110)	$15\times10\times1$	15
	(111)	$10\times10\times1$	15
$InPd_3$	(100)	$12\times12\times1$	15
	(110)	$12\times8\times1$	15
	(111)	$8\times8\times1$	10

S2 Surface energies

Surfaces can be created by dividing an infinite bulk into two parts. The energy needed to cut the bonds and bring the two resulting parts to infinity determines the surface energy. It is worth noticing that the composition of the bulk and the surface can differ. Consequently, the chemical potentials of the single material constituents become involved. The surface energy is calculated by

$$\gamma = \frac{1}{2A}\left(E_{\text{tot}} - \sum_{i=1}^{M} n_i\mu_i\right) \tag{S1}$$

where A is the surface area, E_{tot} is the total energy of the slab made of M elements, n_i is the number of atoms of element i and μ_i its chemical potential. In the case of In-Pd alloy, one obtains:

$$\gamma = \frac{1}{2A}(E_{\text{tot}} - n_{\text{Pd}}\mu_{\text{Pd}} - n_{\text{In}}\mu_{\text{In}}) \tag{S2}$$

The surface atoms are in equilibrium with the bulk, i.e. the underlying bulk alloy. Therefore the chemical potentials μ_{In} and μ_{Pd} are related to the bulk total energy $E^{\text{b}}_{\text{tot}}$:

$$(n^{\text{b}}_{\text{Pd}} + n^{\text{b}}_{\text{In}})E^{\text{b}}_{\text{tot}} = n^{\text{b}}_{\text{Pd}}\mu_{\text{Pd}} + n^{\text{b}}_{\text{In}}\mu_{\text{In}} \tag{S3}$$

where n^{b}_{Pd} and n^{b}_{In} are the number of Pd and In atoms in the corresponding bulk system. Alternatively, the previous relationship can be written as a function of the formation enthalpy ΔH_{f}:

$$(n^{\text{b}}_{\text{Pd}} + n^{\text{b}}_{\text{In}})\Delta H_{\text{f}} = n^{\text{b}}_{\text{Pd}}(\mu_{\text{Pd}} - \mu^{\text{b}}_{\text{Pd}}) + n^{\text{b}}_{\text{In}}(\mu_{\text{In}} - \mu^{\text{b}}_{\text{In}}) \tag{S4}$$

where $\mu^{\text{b}}_{\text{i}}$ is the cohesive energy of the elemental bulks. Thus, in the case of a binary compound, the surface energy can be written as a function of only one chemical potential. In the following, we focus on the one of Pd.

The stability of the surface against segregation implies that the chemical potential μ_{Pd} takes values in the range:

$$\mu^{\text{b}}_{\text{Pd}} - \frac{n^{\text{b}}_{\text{Pd}} + n^{\text{b}}_{\text{In}}}{n^{\text{b}}_{\text{In}}}\Delta H_{\text{f}} \leq \mu_{\text{Pd}} \leq \mu^{\text{b}}_{\text{Pd}} \tag{S5}$$

Thus, when $\Delta\mu_{\text{Pd}} = \mu_{\text{Pd}} - \mu^{\text{b}}_{\text{Pd}} = 0$, the surface energy is written:

$$\gamma = \frac{1}{2A}[E_{\text{tot}} - n_{\text{Pd}}\mu^{\text{b}}_{\text{Pd}} - \frac{n_{\text{Pd}}}{n^{\text{b}}_{\text{Pd}}}((n^{\text{b}}_{\text{Pd}} + n^{\text{b}}_{\text{In}})E^{\text{b}}_{\text{tot}} - n^{\text{b}}_{\text{Pd}}\mu^{\text{b}}_{\text{Pd}})] \tag{S6}$$

Alternatively, when $\Delta\mu_{\text{Pd}} = \mu_{\text{Pd}} - \mu^{\text{b}}_{\text{Pd}} = \frac{n^{\text{b}}_{\text{Pd}} + n^{\text{b}}_{\text{In}}}{n^{\text{b}}_{\text{In}}}\Delta H_{\text{f}}$ the surface energy becomes:

$$\gamma = \frac{1}{2A}[E_{\text{tot}} - n_{\text{In}}\mu^{\text{b}}_{\text{In}} - \frac{n_{\text{In}}}{n^{\text{b}}_{\text{In}}}((n^{\text{b}}_{\text{Pd}} + n^{\text{b}}_{\text{In}})E^{\text{b}}_{\text{tot}} - n^{\text{b}}_{\text{In}}\mu^{\text{b}}_{\text{In}})] \tag{S7}$$

We have performed DFT calculations of In-Pd surface of varying orientation and composition. In particular, we have investigated

[a] Université de Lorraine, CNRS, Institut Jean Lamour, UMR 7198, Campus Artem, 2 allée André Guinier, F-54011, Nancy, France; [b] Department of Chemistry and Materials Science, Aalto University, 02150 Espoo, Finland; Department of Applied physics, Aalto university, Espoo, Finland; [c] Université Paris-Saclay, CEA, Service de Recherches de Métallurgie Physique, 91191, Gif-sur-Yvette, France
E-mails: alexis.front@aalto.fi; emilie.gaudry@univ-lorraine.fr

In_3Pd_2, InPd and $InPd_3$ surface compounds. From equations (S6) and (S7), we have computed surface energy upon variation of the Pd chemical potential. Values of surface energies at the In-rich and Pd-rich limits are gathered in Tab. S2.

Table S2 Surface energies (J/m^2) of several orientations for In_3Pd_2, InPd and $InPd_3$

	(hkl)	label	$\Delta\mu_{Pd} = 0$	$\Delta\mu_{In} = 0$
In_3Pd_2	(110)	1	0.767	0.767
	(101)	2	1.191	0.595
	(101)	3	0.861	1.457
	(100)	4	0.930	0.685
	(100)	5	0.994	0.994
	(001)	6	0.663	1.344
	(001)	7	1.472	0.791
InPd	(111)	8	1.112	0.721
	(111)	9	0.687	1.146
	(110)	10	0.738	0.738
	(100)	11	0.930	1.406
	(100)	12	1.666	0.670
$InPd_3$	(111)	13	1.047	1.047
	(110)	14	1.206	1.343
	(100)	15	1.072	0.491

S3 Bond analysis

In addition to the analysis presented in section 2.3 (see main paper), we performed a detailed pair energy analysis using the chemically ordered and disordered NPs. Our objective was to quantify the energy balance of given ij pairs. Thus, we introduced the following quantity:

$$\left\langle \tilde{\mathcal{V}}_i' \right\rangle (r_b) = \frac{1}{r_b} \sum_{j=1}^{M} \int_0^{r_b} \left\langle N_{ij} \tilde{V}_{ij} \right\rangle (r_b') dr_b', \tag{S8}$$

where $\left\langle N_{ij} \tilde{V}_{ij} \right\rangle (r_b')$ is the radial average, for a given radius r_b', of the pseudo-pairwise electrostatic potential between species i and j $\left(\tilde{V}_{ij}\right)$ weighted by the number of interaction between i and j pairs $\left(N_{ij}\right)$. The integer M is the total number of species in the system. The quantity $\left\langle \tilde{\mathcal{V}}_i' \right\rangle (r_b)$, computed for a given radius (r_b), and a given species i, is positive and negative when integrated interactions are averagely repulsive and attractive, respectively.

Fig. S3 gathers the results of our balance pair interactions analysis, performed on small Pd-rich Wulff Polyhedra nanoparticles ($D = 24$ Å) of In_3Pd_2 (left), InPd (middle), $InPd_3$ (right). We represent the contribution from In-In bonds in brown and in blue for Pd-X bonds (X = In, Pd). The upper row displays ordered WP_{Pd} whereas the bottom row represents disordered WP_{Pd}. We carried out this procedure for non-relaxed NPs (Fig S3 (A)) and for NPs after structural relaxation (Fig S3 (B)). Integrated results are smoothed by using cubic splines. We renormalised integrated pair energies by $|||\left\langle \tilde{\mathcal{V}}_i' \right\rangle|||_\infty$ (where $\|\cdot\|_\infty$ is the infinity norm). Values of the renormalisation factor are given in Fig. S3.

We can notice that for almost all NPs, integrated interactions involving In-In pairs are larger than those involving Pd atoms. According to $\left\langle \tilde{\mathcal{V}}_i' \right\rangle (r_b)$, interactions with Pd tend to stabilise NPs structures for any composition and any type (chemically ordered or disordered NPs, blue lines in Fig. S3). In the case of $InPd_3$ NPs (right column in Fig. S3), In-In integrated pair interactions (brown lines) are negative. This stabilising behavior is observed for ordered and disordered NPs but also for relaxed and non relaxed structures. Thus, balance interactions tend to preserve the crystalline character of $InPd_3$ NPs. Results for In_3Pd_2 and InPd NPs are qualitatively and quantitatively different (left and middle columns, in Fig. S3). In the case of **relaxed** NPs – chemically ordered or disordered NPs (Fig. S3B) – integrated In-In interactions are slightly negative for $r_b \simeq 3.0$ Å, i.e. for short range interactions. We can then conclude that In_3Pd_2 and InPd NPs are stabilised by these short range interactions. This behavior is also observed for ordered In-rich NP where integrated In interactions are slightly negative at short range. In chemically disordered In_3Pd_2 and InPd NPs (bottom rows), the integrated In-In interactions are repulsive at short range. This repulsive behavior induces huge structural changes close to In atoms in order to recover an attractive interactions balance. Huge local change in NPs structures tend to an amorphisation behavior.

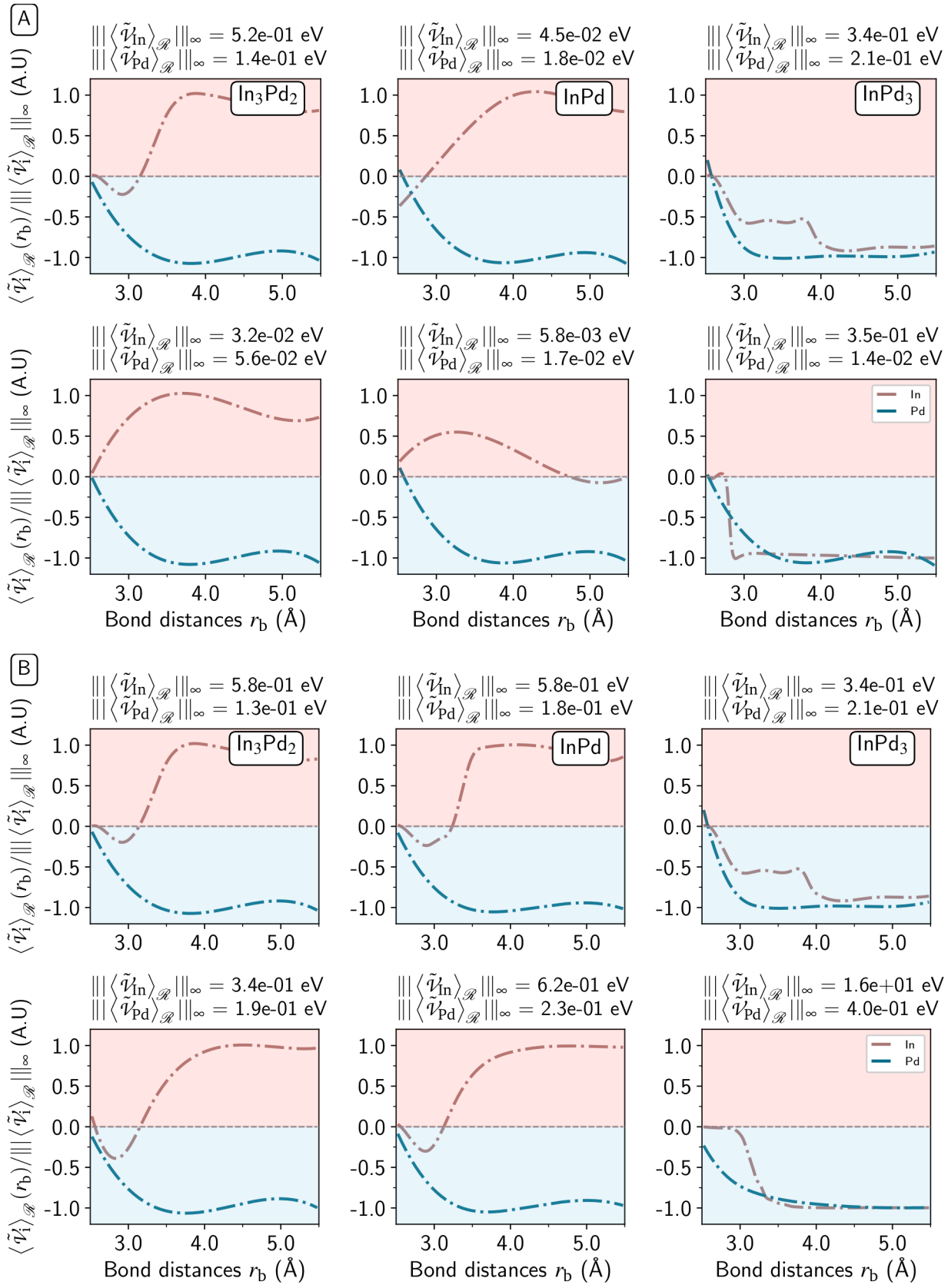

Table S3 Integrated pair energies $\langle\tilde{\nu}_i\rangle(r_b)$ as a function of the bond distances of small WP_{Pd} nanoparticles ($D = 24$ Å), built from the In_3Pd_2 (left), InPd (middle), $InPd_3$ (right) compounds. We represent In-In and In-Pd bonds in brown and in blue, respectively. The upper and bottom rows display ordered and disordered WP_{Pd}, respectively. Analysis have been performed for non-relaxed NPs in Fig S3 (A) and for NPs after structural relaxation in Fig S3 (B). Integrated results are smoothed by cubic splines. We renormalised the integrated pair energies by $|||\langle\tilde{\nu}_i\rangle|||_\infty$. Values of the renormalisation factors are given above each subfigure.

S4 Work-functions

he work-functions are computed based on the radial averaged potential energy function ($\langle V_{\mathrm{LP}}\rangle(r,\delta r)$) computed by :

$$\langle V_{\mathrm{LP}}\rangle(r,\delta r)=\frac{1}{\int_{\mathbb{R}^3_+}\mathbb{1}_{|r-\|\mathbf{r}'\||\leq\delta r}d\mathbf{r}'}\int_{\mathbb{R}^3_+}V_{\mathrm{LP}}(\mathbf{r}')\mathbb{1}_{|r-\|\mathbf{r}'\||\leq\delta r}d\mathbf{r}', \quad \text{(S9)}$$

Practically, we set $\delta r=\sqrt{\sum_{i=1}^{3}\|\mathbf{a}_i/N_i^k\|^2}$ where $\mathbf{a}_i$ are the vectors of the simulation box and N_i^k the numbers defining the discrete FFT grid along the $\mathbf{a}_i/\|\mathbf{a}_i\|$ direction.

Table S4 Work-functions of NPs (see Fig. 8) and surfaces. The size of NPs are given (N, number of atoms in the NP) as well as their global and surface Pd content (in at. %) respectively $c_{\mathrm{Pd}}^{\mathrm{NP}}$ and $c_{\mathrm{Pd}}^{\mathrm{surf}}$.

	Morphology	N	$c_{\mathrm{Pd}}^{\mathrm{NP}}$	$c_{\mathrm{Pd}}^{\mathrm{surf}}$	WF (eV)
In	(101)		-	0.0	3.670
In_3Pd_2	Oh*	363	0.435	0.392	4.073
	Oh*	1143	0.397	0.345	4.117
	Cu*	411	0.443	0.423	4.065
	Cu*	831	0.387	0.308	4.091
	WP_{Pd}	381	0.394	0.320	4.116
	WP_{Pd}	1125	0.395	0.383	4.072
	WP_{In}	381	0.346	0.327	3.973
	WP_{In}	757	0.375	0.372	4.073
	(101)	5	-	0.4	4.4356
InPd	Oh*	385	0.540	0.550	4.139
	Oh*	1017	0.517	0.500	4.130
	Cu*	379	0.485	0.505	4.141
	Cu*	1145	0.503	0.496	4.194
	WP_{Pd}	369	0.499	0.480	4.498
	WP_{Pd}	1105	0.500	0.491	4.528
	WP_{In}	387	0.475	0.304	4.169
	WP_{In}	1131	0.509	0.539	4.324
	(100)	2	-	0.5	4.482
$InPd_3$	Oh	489	0.736	0.770	4.487
	Oh	885	0.746	0.758	4.515
	Cu	309	0.658	0.495	3.931
	Cu	1139	0.688	0.497	4.536
	WP_{Pd}	405	0.770	0.824	4.526
	WP_{Pd}	1289	0.735	0.697	4.466
	WP_{In}	365	0.658	0.495	3.931
	WP_{In}	1099	0.688	0.497	4.054
	(100)	4	-	0.5	4.412
	(111)	4	-	0.75	4.762
Pd	(111)		-	1.0	5.210

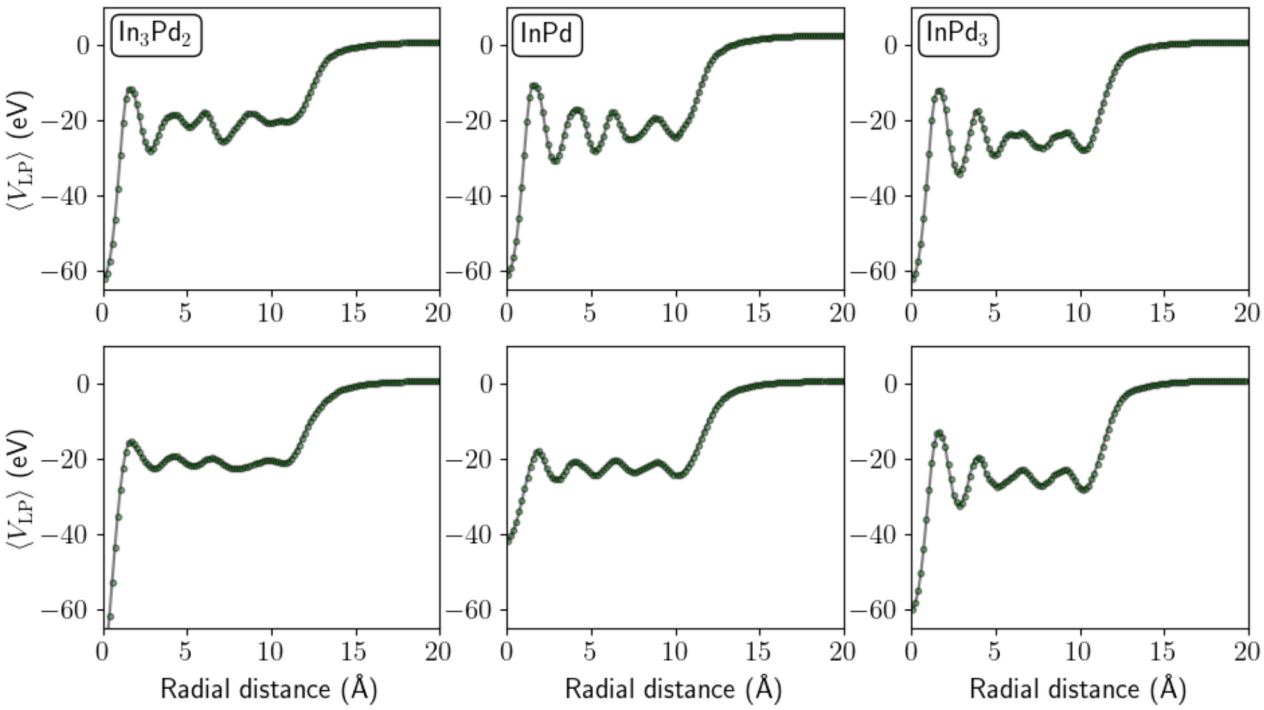

Fig. S1 Radial averaged potential energy for small Pd-rich Wulff Polyhedra nanoparticles (diameter 24 Å) of In_3Pd_2 (left), InPd (middle), $InPd_3$ (right) compounds. The upper row displays ordered WP_{Pd} whereas the bottom row represents disordered WP_{Pd}.

S5 Benchmark of work-functions calculation methodology

In order to validate our new methodology, we sought reference experimental data on metallic NPs. Literature on NPs work function measurement is still extremely limited. We choose to benchmark our NPs' work-function calculations on gold NPs. Our *ab initio* results are directly compared with recent experimental data extracted from Zhang *et al.*[1].

We generated several gold NPs presenting different morphologies (Wulff polyhedron, decahedron and icosahedron) and different sizes (from 200 to 800 atoms). We used the `VASP` [2–4] software to perform electronic structure calculation. We used the projector augmented wave (PAW) method,[5,6] the generalised gradient approximation (GGA-PBE),[7,8] and an energy cutoff set to 300 eV. Eleven valence electrons have been explicitly treated for Au ($5s^1 4d^{10}$). Total energies have been minimised until the energy differences became less than 10^{-5} eV between two electronic cycles. Atomic structures have been relaxed till the Hellmann-Feynman forces were as low as 0.02 eV/Å. Then our work-function methodology is performed. Effective NP sizes are estimated from the work-function decreasing. This size estimation takes into account the geometrical size of NP but also the "electronic skin" at the NP surface. Actually, these two contributions are taken into account experimentally in Kelvin probe microscopy.

In their paper, Zhang *et al.*[1] were able to measure precisely NPs' work-function for sizes greater than 4.0 Å. Our calculations allow us to compute work-function for range of size between 2.0 Å and 4.0 Å. Zhan *et al.* performed their measurements on gold NPs in interaction with Si substrate. This interaction induces an inherent shift in WF which can not be directly estimated from our *ab initio* calculation. To avoid this bias we first fitted experimental and numerical WF data with the following function (the function form is based on analytical analysis given by Zhang *et al.*[1]) :

$$W_{\mathrm{NP}}(s) = \frac{\alpha}{s} + \lim_{s\to\infty} W_{\mathrm{NP}}(s), \tag{S10}$$

where s is the NP size in Å and α is a fitting parameter in eV.Å. W_{NP}^{∞} is the value of WF when the size of the NP tends towards infinity. By subtracting the $\lim_{s\to\infty} W_{\mathrm{NP}}(s)$ term for both (experimental and numerical data) we can make the direct comparison. Comparison between experimental and numerical gold NP work-function are presented in figure 10.

Based on gold NPs work function benchmark, we consider that our methodology can be used for more complex system like InPd NPs. We keep in minds that our procedure can present a systematic error comparing to experimental data. Nevertheless, based on gold NPs benchmark, this systematic error only depends on a constant shift that can be numerical estimated (see our fitting procedure). Moreover, our methodology is able to well reconstruct the variation of work function depending on the NPs size.

S6 Formation enthalpies

The formation enthalpies of NPs considered in the paper are given in Tab S5

Table S5 Formation enthalpies of nanoparticles considered in this work.

	Morphology	N	Formation enthalpy (eV/at.)
In_3Pd_2	Oh*	363	-0.911
	Oh*	1143	-0.966
	Cubo*	411	-0.938
	Cubo*	831	-0.931
	WP_{Pd}	381	-0.865
	WP_{Pd}	1125	-0.978
	WP_{In}	381	-0.819
	WP_{In}	757	-0.927
InPd	Oh*	385	-0.919
	Oh*	1017	-1.094
	Cubo*	379	-1.029
	Cubo*	1145	-1.123
	WP_{Pd}	369	-1.087
	WP_{Pd}	1105	-1.172
	WP_{In}	387	-1.019
	WP_{In}	1131	-1.135
$InPd_3$	Oh	489	-1.281
	Oh	885	-1.332
	Cubo	309	-1.260
	Cubo	1139	-1.341
	WP_{Pd}	405	-1.244
	WP_{Pd}	1289	-1.389
	WP_{In}	365	-1.252
	WP_{In}	1099	-1.365

Notes and references

1 Y. Zhang, O. Pluchery, L. Caillard, A.-F. Lamic-Humblot, S. Casale, Y. J. Chabal and M. Salmeron, *Nano Letters*, 2015, **15**, 51–55.

2 G. Kresse and J. Hafner, *Physical Review B*, 1993, **47**, 558–561.

3 G. Kresse and J. Furthmüller, *Computational Materials Science*, 1996, **6**, 15–50.

4 G. Kresse and J. Furthmüller, *Physical Review B*, 1996, **54**, 11169–11186.

5 P. E. Blöchl, *Physical Review B*, 1994, **50**, 17953–17979.

6 G. Kresse and D. Joubert, *Physical Review B*, 1999, **59**, 1758–1775.

7 J. P. Perdew, K. Burke and M. Ernzerhof, *Phys. Rev. Lett.*, 1996, **77**, 3865.

8 J. P. Perdew, K. Burke and M. Ernzerhof, *Phys. Rev. Lett.*, 1997, **78**, 1396.

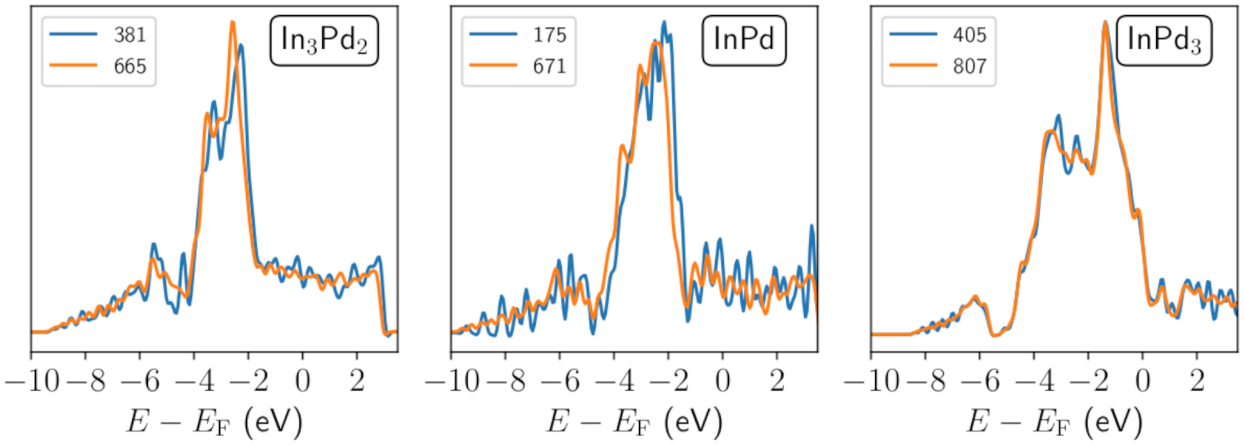

Fig. S 2 Density of states of two sizes of Wulff Polyhedra Pd-rich (WP_{Pd}), built from In_3Pd_2, InPd an $InPd_3$ bulk compounds.